JOURNAL OF MATERIALS SCIENCE 21 (1986) 2224–2238

Review
Rapidly solidified titanium alloys for high-temperature applications

SUNG H. WHANG*
Barnett Institute of Chemical Analysis and Materials Science, Northeastern University, Boston, Massachusetts 02115, USA

The application of rapid solidification technology (RST) to titanium alloy systems is relatively new and became the subject of active research since it was demonstrated that novel titanium alloys of higher temperature capability can be synthesized through new alloy design based on rapid solidification processing. The effects of rapid solidification on the occurrence of metastable phases, microstructures and mechanical properties in binary and ternary titanium alloys are reviewed. In particular, earlier results from RS α-Ti alloy research have shown that many different novel dispersoids, some of which are coarsening-resistant at elevated temperatures (600 to 800° C), can be created in the matrix through RST. The alloys containing novel dispersoids also exhibit good creep resistance at elevated temperatures. Further studies on α/β- and β-Ti alloys through RST, in conjunction with the development of various processing technologies for bulk alloy manufacturing, are clearly desirable.

1. Introduction

Historically, the development of high-temperature titanium alloys dates back to the 1960s when titanium alloys were largely strengthened by silicon in order to provide adequate creep strength at elevated temperatures [1–4]. Furthermore, zirconium and molybdenum were added to strengthen the matrix and stabilize silicide dispersion. These zirconium- and silicon-containing alloys have been optimized with respect to creep strength and other structure-sensitive properties for use in a temperature range of 500 to 600° C [5], slightly larger than the 0.4 homologous melting temperature. In fact, this homologous temperature of titanium alloys for pratical application is much lower than that of superalloy, where maximum temperatures can reach as high as 0.9 homologous temperature. The fact that conventional titanium alloys do not have high-temperature capability has motivated the development of high-temperature titanium alloys.

Nevertheless, there a number of stumbling blocks to the development of higher temperature (> 600° C) titanium alloys. The identified obstacles are: (i) no coherent and stable precipitate at high temperatures, similar to γ' in superalloy, was found in titanium alloy systems; (ii) at temperatures above the α transus temperature, the silicide coarsening rate is very high, due to the high diffusivity of the silicon solute [6]; (iii) a rapid oxidation reaction occurs above 600° C, seriously challenging high-temperature applications [7, 8]. As a result, some efforts have been directed toward (a) increasing the allotropic temperature via alloying with strong alpha-stabilizing elements; (b) introducing precipitates or dispersoids other than silicides into the matrix through rapid solidification processing (RSP) [9–11]; and (c) applying oxidation-resistant coatings to the alloy surface.

Alternatively, there have been a number of attempts to replace α-Ti alloy with titanium intermetallic compounds for high-temperature applications [12–18], i.e. the titanium aluminides TiAl and Ti_3Al. These aluminides have good oxidation resistance and high moduli, but they have poor ductility as well as poor formability, thus limiting the practical use of these aluminides at high temperatures [12]. Nevertheless, efforts have been made to improve the ductility of these aluminides at high temperature by introducing various alloying elements into the aluminides [16].

A recent approach to high-temperature titanium alloy development is mainly to create fine and stable dispersoids in the titanium matrix through RSP. Additive elements include metalloids (boron, carbon, silicon), rare earth metals (yttrium, lanthanum, cerium, neodymium, erbium, etc.) and an actinide element (thorium). By and large, all these elements have negligible solubility in titanium at room temperature, but dissolve in titanium to a limited amount at high temperatures. Furthermore, these elements form stable dispersoids in the titanium matrix, providing dispersion-strengthening at elevated temperatures. Previously, a significant amount of rare-earth metals (~ 1 at %) was dissolved into titanium through the ingot metallurgy process [19–22], but the resulting alloy phase contained coarse rare-earth particles

Present address: Department of Metallurgy and Materials Science, Polytechnic University, 333 Jay Street, Brooklyn, New York 11201, USA.

0022–2461/86 $03.00 + .12

ranging from one to several micrometres in diameter in the as-cast ingot [22]. Furthermore, development of high-temperature titanium alloy by the addition of rare-earth metals through the ingot metallurgy technique appeared to be at an impasse in the presence of such coarse particles. The recent advent of rapid solidification technology (RST) has restored research interest in titanium alloys with rare-earth addition, since the formation of such coarse particles is prevented and fine and uniform particles are created. Although the possiblity of developing high-temperature alloys applicable at the temperature range of 600 to 800° C has been demonstrated, measures must be taken in order to prevent severe surface oxidation at these temperatures. In this regard, research on rapidly solidified titanium alloys for high-temperature applications is still in the experimental stage, and further property evaluation for practical applications is needed.

This paper reviews the research in rapidly solidified titanium alloys in the last ten years.

2. Rapid solidification processing of titanium alloys

Despite rapid progress in RSP technology over more than a decade, the full-scale development of titanium alloys through RSP has been hindered by the reaction of titanium with crucible materials and with the environment. Although many alloy powder processes for near-net shape titanium metallurgy have emerged in the 1970s, the methods neither intend to nor do they produce a high quench rate ($> 10^3$ K sec^{-1}) during the powder production. For example, the rotating electrode process (REP) [23] produces titanium alloy powder of mean diamter 175 μm in an argon atmosphere. The estimated cooling rate based on the microstructure observation does not exceed 10^3 K sec^{-1} [24]. Hence, it is considered a conventional processing technique.

In parallel, during the last decade, the melt-extraction techniques have been developed for quenching titanium alloys into fibres [25, 26]. Added recently were arc melt-spinning [10, 27], laser spin atomization [28], electron-beam melting/splat quenching [9, 29], and ultrasonic gas atomization [9]. The pendant drop melt-extraction techniques produce so-called L/D powder, or C- D- and L-shaped fibres of Ti–6Al–4V, and other heavily alloyed titanium materials such as Ti–5.4Al–3.6V–8Fe–3Cu [30]. The melt-extraction techniques provide contamination-free fibres when processed in a vacuum chamber. Lab-scale as well as pilot-scale arc melt-spinning technique has been used in producing titanium alloy ribbon of amorphous and microcrystalline forms [10, 27]. This technique adopts the combination of a water-cooled cold copper crucible with an arc heating scheme that uses non-consumable tungsten electrodes under an argon atmosphere. As a result, titanium alloy ribbons or flakes processed by this technique are also contamination-free, since they are melted in the cold copper crucible and spun in an inert gas atmosphere. The ribbon produced has a uniform thickness of 20 to 50 μm.

2.1. The melt-extraction process

The first attempt to produce fine fibres or filaments of metals and alloys in a clean environment was made by this technique. There are two methods of melt-extraction procedure: crucible melt-extraction and pendant drop melt-extraction (PDME) (Fig. 1a) [26]. In the former, a rotating copper disc with a sharp peripheral angle, immersed in the melt, drags out metal filaments from the melt. The fibre shape depends upon the immersion depth and the speed of the disc. The shapes include D (Fig. 1b), C, and L.

Although the surface of the melt is covered with slag, this technique was used primarily for non-reactive metals such as iron, steel and aluminium. The second technique, pendant drop melt-extraction, may be regarded as a non-crucible melt-spinning technique. Titanium alloy rod hanging above the spinning disc is heated to melt by an electron beam, a laser beam or some clean heat source. The thickness (d) of the fibre produced in this technique is expressed with an empirical relation [30]

$$d = CV^{-1/2}$$

where C and V are a proportionally constant and the surface velocity of the disc, respectively. It should be noted that the exponent, 0.5, is half the figure in

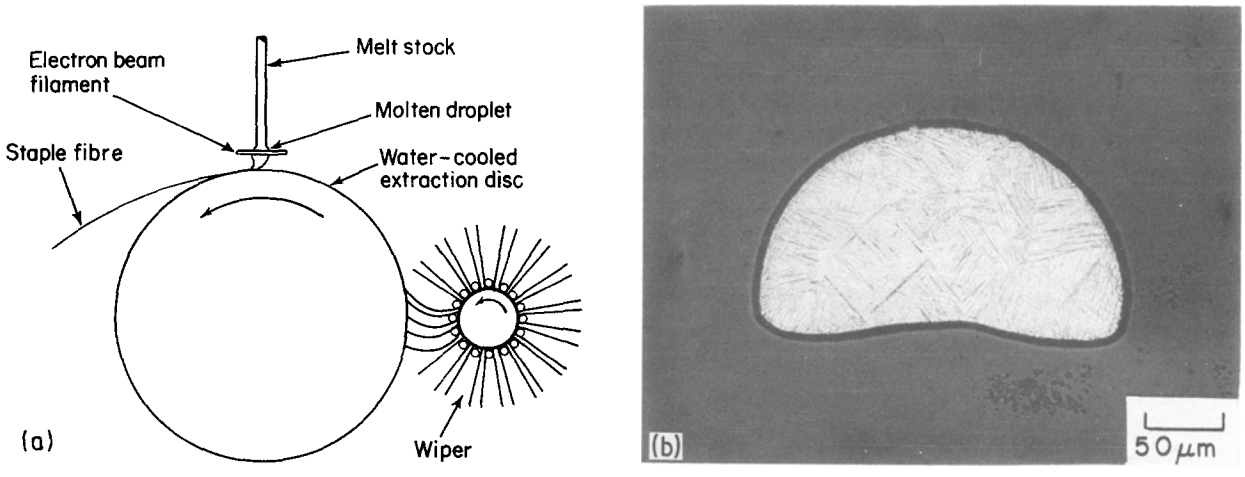

Figure 1 Pendant drop melt-extraction process [26]: (a) schematic drawing, (b) D-shape fibre product. Photo courtesy of Dr R. E. Maringer, Battelle Columbus Labs.

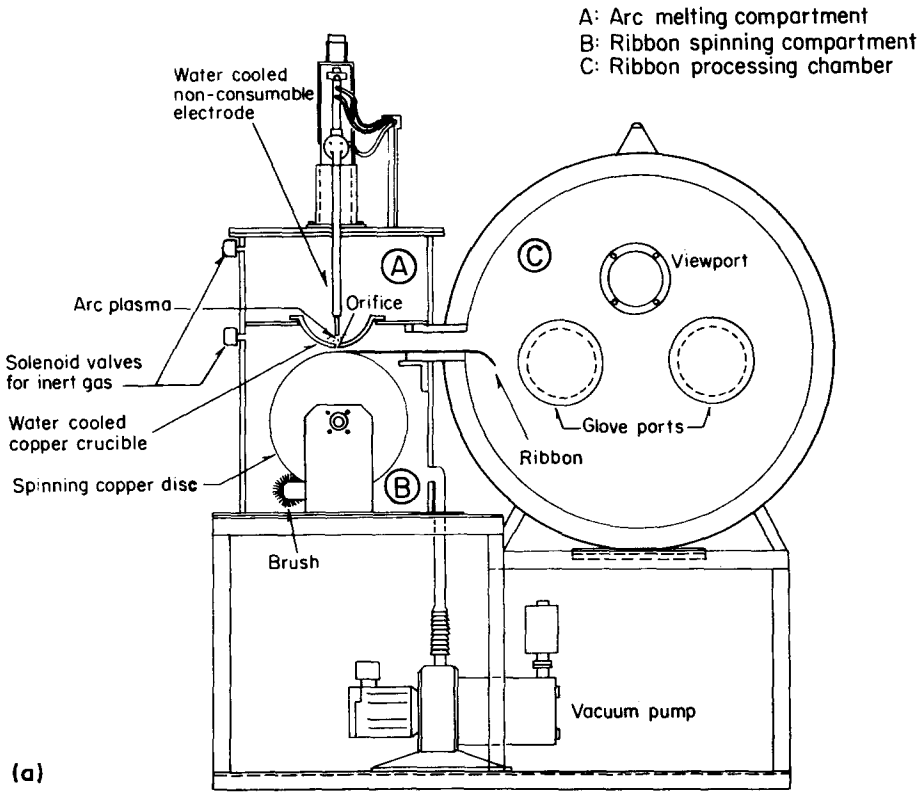

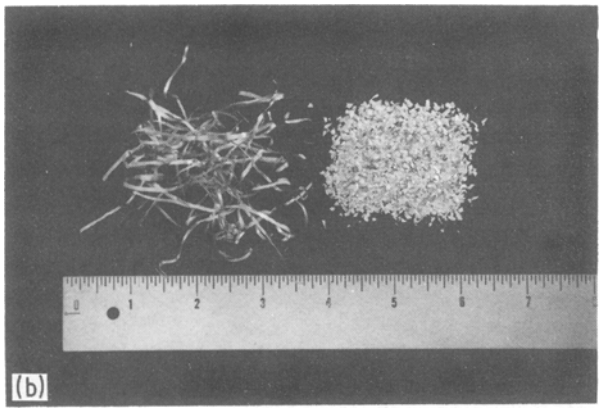

Figure 2 Arc melt spin process: (a) schematic drawing of arc melt-spinning unit, (b) produced ribbon and chopped ribbon powder.

ordinary melt-spinning, ~1.0 [31, 32]. Under well-controlled processing conditions, titanium alloy fibre of ~58 μm thick has been produced at an estimated cooling rate of ~10^5 K sec^{-1}. Also, melt-extraction techniques are able to produce short fibres of a length-to-diameter ratio of 20 : 1 using a notched disc. These flakes, so-called L/D powder, are amenable to direct compaction and consolidation without further reduction in size, i.e. cutting or chopping. In electron-beam melting/splat quenching [29], similar to PDME, the molten droplet produced from titanium alloy stock by electron-beam heating falls on to the face of the spinning disc and produces a shallow U-shaped flake, i.e. a boomerang-shaped flake.

2.2. Arc melt-spinning

In contrast to the ordinary melt-spinning technique [10, 27, 33], in which various crucibles (quartz tubing, clay, ceramic) are used to melt metals and alloys by induction or resistant heating, the arc melt-spinning technique (AMS) uses a cold copper crucible with an orifice and arc eletrode to melt-spin alloys. The molten alloy is injected through the orifice of the copper crucible by the gas pressure differential betweeen the melting and spinning compartments (Fig. 2a). The ribbon and the chopped flake produced by the rotary-blade ribbon cutter are shown in Fig. 2b. This melt-spin technique has advantages over other techniques in that (a) uniform and thin ribbon of reactive alloys as well as refractory alloys (niobium, tantalum, molybdenum, tungsten) can be produced without contamination; and (b) the molten jet can be shaped into a desired geometry and spun into a relatively thin sheet (20 to 50 μm thick), providing a high cooling rate (5×10^5 to 10^7 deg sec^{-1}). Many α-Ti alloys containing rare-earth metals have been processed into ribbon materials by this technique.

2.3. Atomization

In centrifugal atomization [28, 29], the surface tension of the molten alloy becomes an important intrinsic parameter for the effectiveness of the atomization, since the surface tension opposes the centrifugal force which breaks the molten alloy into fine droplets: i.e. the higher the surface tension, the stronger the centrifugal force required. The surface tension of a molten alloy decreases linearly with the melt temperature, whereas it changes radically with a small amount of a particular additive element [34]. Based on the balance between the surface tension against the centrifugal force, the following relation was derived [23]:

$$r = \frac{(1.5)^{1/2}}{\omega}\left(\frac{\sigma}{R\varrho}\right)^{1/2}$$

where r, ω, R, σ and ϱ are the radius of droplet, angular velocity and radius of spinning rod, surface

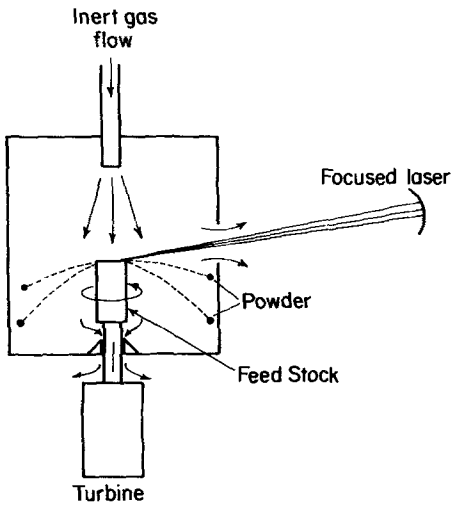

Figure 3 Schematic drawing of laser melt-spin atomizer [9].

tension, and density, respectively. In the centrifugal atomization, the rotational velocity to overcome the surface tension of the melt, N (r.p.m.), is proportional to $\sigma^{1/2}$.

Fig. 3 shows a schematic diagram of a laser melt-spin atomization unit. In this technique, an extruded titanium alloy rod, melted by a laser beam at one end, rotates at a speed up to 35 000 r.p.m., generating various mean sizes of spherical powder depending upon the rotational speed. The powder produced, Ti–6Al–4V, reportedly has an average particle distribution ranging from 0.1 to 0.65 mm diameter, with a corresponding rotating speed from 303 to 838 rad sec^{-1} or 8000 to 29 000 r.p.m. as shown in Fig. 4a (3 cm rod diameter) and Fig. 4b (1.5 cm rod diameter) [29]. It is apparent from this report that the rotational speed of the rod should increase far beyond 60 000 r.p.m. in order to produce an average powder size of $\sim 75\,\mu m$ diameter, provided the relation given above is correct.

Rapidly solidified alloy powder has also been produced by an ultrasonic gas atomizer using a

TABLE I Processing techniques and their cooling rates (inert gas environment)

Technique	Shape and size	Estimated cooling rate ($K\,sec^{-1}$)
Hammer and anvil (HA)	Foil 10 to 50 μm	10^6 to 10^7
Pendant drop melt-extraction (PDME)	Fibre: 0.025 to 0.125 mm	10^3 to 10^5
Arc melt-spinning (AMS)	Ribbon 15 to 50 μm	10^5 to 10^6
Laser spin atomization	Spherical powder 100 to 650 μm	10^2 to 10^4

zirconia crucible with rare earth oxide [29]. The gas stream of supersonic velocity (Mach 2 to 2.5), a pulse frequency of 100 kHz, and a pressure 8.3 MPa, strikes the molten jet at a shallow angle ($\sim 22.5°$). The resulting powder has a spherical shape from 10 to 100 μm diameter. This technique requires special care of the coating materials, which are easily damaged during operation. The stability of the coating at high temperature, and its chemical reaction with titanium, will be the main concern in this technique. Typical processing techniques and corresponding cooling rates are summarized in Table I.

A large difference in cooling rate is observed between the various techniques. For example, the cooling rate of atomized powder was determined by measuring the dendrite arm spacing in Ti–15V–3Al–3Sn–3Cr [29]. A plot of the particle diameter (D) of laser melt-spin atomized powder against cooling rate, estimated from the dendrite arm spacing, yields a linear correlation on a log–normal plot. The slope in the plot ($\dot{T}$ against D) is roughly -2 [29], which is in agreement with ideal cooling, but in disagreement with Newtonian cooling [28, 31, 35], where the slope is -1. Such deviation cannot be accounted for, since sufficient information is not available.

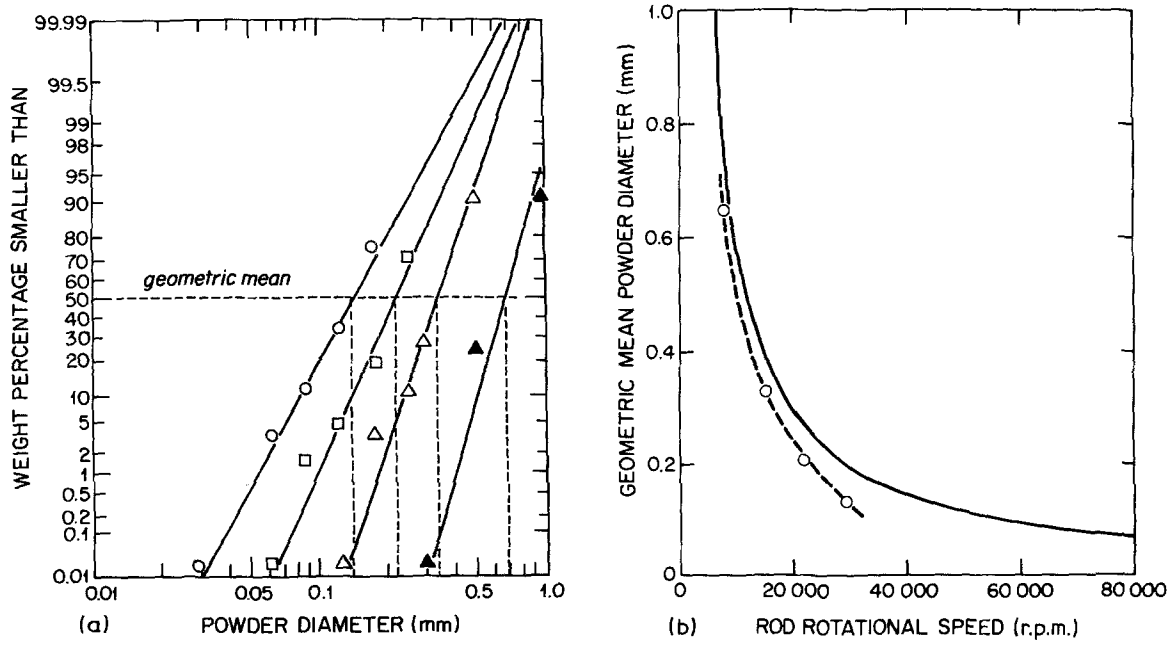

Figure 4 Particle size distribution of Ti–6Al–4V alloy [29]: (a) powder diameter against accumulative weight percentage; (b) powder diameter against rod rotation speed. Rod diameter 1.5 cm.

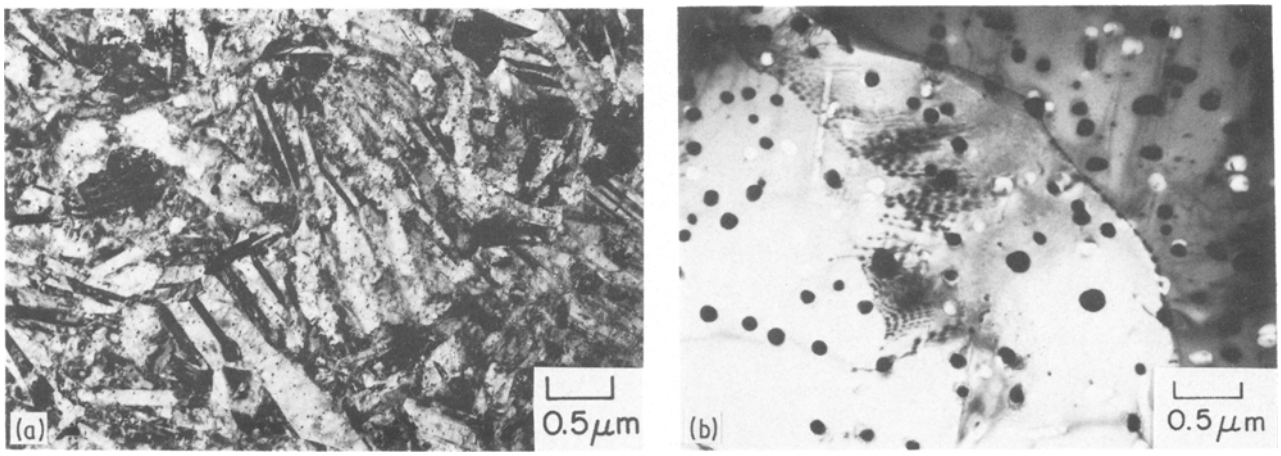

Figure 5 TEM micrographs of Ti–5Al–4.5La alloy: (a) as-splat foil by the hammer–anvil technique; (b) as-quenched ribbon by arc melt-spinning technique.

For another example, a ternary alloy containing a rare-earth metal (Ti–5Al–4.5La) when quenched by the hammer–anvil (HA) technique (Fig. 5a) reveals fine martensitic structure combined with precipitates of 5 nm diameter; the same alloy composition by AMS techniques shows a particle size of 50 to 200 nm diameter (Fig. 5b) [36]. Similarly, binary Ti–(5.9 to 7.9) Ni alloys processed by PDME and electron beam melting/splat quenching (EBSQ) show beta eutectoid decomposition, while splat alloy by the HA technique does not indicate such decomposition. This fact suggests that at the break-off point from the copper disc, the temperature of the alloy ribbon is high, possibly above 750° C (Fig. 6) [37].

On the other hand, $Ti_{60}Ni_{30}Si_{10}$ ribbon has been routinely melt-spun into glassy alloy by AMS techniques, indicating that the alloy temperature at the break-off is below the first crystallization temperature of this alloy, i.e. 470° C [38]. These conflicting results demonstrate a large variation in cooling rates, depending on composition, additive elements, processing techniques and other processing parameters. A systematic investigation is due, in order to further understand the relationship between the cooling rate and processing variables.

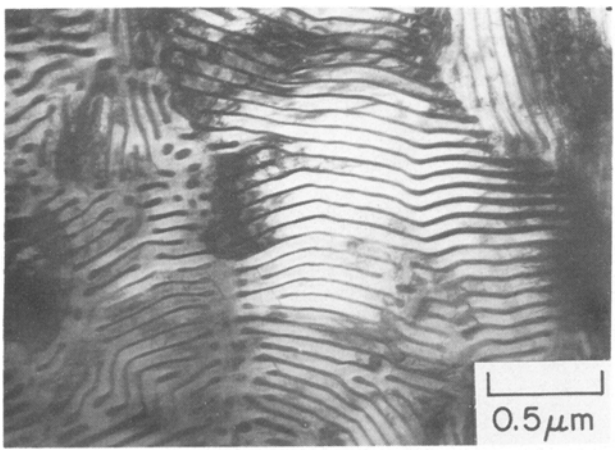

Figure 6 TEM micrograph of Ti–7.9Ni fibre by pendant drop melt-extraction [37]. Photo courtesy of Drs S. S. Krishnamurthy and F. H. Froes, Air Force Wright Aeronautical Labs.

3. Consolidation

Since powder products from rapidly solidified materials take various shapes, size distributions and surface conditions, depending upon the processing techniques, the consolidation and thermomechanical processing of the powders requires different consolidation conditions. It is often found that improvement in powder bonding and coarsening of powder microstructure occurs simultaneously with annealing. Preliminary studies on optimization of these conditions with respect to mechanical properties have been carried out.

In earlier work, rapidly quenched Ti–6Al–4V flakes produced by the pendant drop melt-extraction technique were vacuum hot-pressed at 955° C one hour under a pressure of 5.5 MPa [26]. Alternatively, the same flakes were cold-pressed under a pressure of 345 MPa and canned in a seamless steel tubing, followed by outgassing at 870° C for 15 h. Hot isostatic pressing (HIP) of the canned powder was performed at 995° C under 167 MPa. Alloys consolidated by both methods yield essentially 100% density, but develop grain growth during high-temperature consolidation.

Since microstructural coarsening during consolidation becomes a critical factor for high-temperature strengthening in dispersion strengthened RS titanium alloy, current consolidation schemes for RS titanium alloys are focused primarily on preventing microstructure coarsening while achieving full densification. In order to achieve both objectives, consolidation techniques that allow low working temperatures are employed. For example, titanium flakes processed by electron beam melting and splat quenching were vacuum hot-pressed at 800 to 950° C under 50 to 100 MPa. Subsequently, the flakes were forged at 800° C into 4.0 μm thick plates and hot-rolled at 800° C into 1.5 μm thin sheets [29]. The flakes (~ 1 to 2 mm long × ~ 1 to 2 mm wide) produced by the arc melt-spinning process were HIPed at 850° C for 3 h at 2.1 GPa using a mild steel can [36]. The consolidated alloy shows full density and good bond character. (Fig. 7 shows typical ribbon, chopped flake, and HIPed alloy.) All these temperatures used for the dispersion-strengthened alloys are roughly 100° C lower than conventional consolidation temperatures.

Figure 7 HIPed Ti–5Al–4.5La alloy from arc melt-spin ribbon.

One of the attractive aspects of titanium alloy consolidation is that the surface oxides of precursor alloys dissipate from the surface of the powder by diffusion during hot consolidation.

4. Microstructural observations

The microstructural characteristics of rapidly quenched titanium alloys have been examined in two states: as-quenched and heat-treated, as in hot consolidation and thermomechanical processing. The microstructure of the as-quenched state is characterized by supersaturation of solute atoms, and refined microstructures consisting of β-grain, acicular α-grain, martensitic structure, precipitate, etc. Heat-treated alloys undergo further changes in microstructure toward the next metastable state or equilibrium state. Despite consolidation and thermomechanical processing, a significant portion of microstructural refinement can be retained in the final product, depending upon the thermal history of consolidation and thermomechanical processing. As a result, microstructures of bulk alloy consolidated from rapidly solidified materials are an order of magnitude finer than those seen in conventional ingot titanium alloys. In particular, the coarsening of rare-earth dispersoid titanium alloys is minimal upon reduced temperature consolidation and deformation.

4.1. Solid solubility of solute

One of the benefits of RS titanium alloy is the increase in solid solubility upon rapid quenching; this permits almost every additive element to dissolve into solid solution or form clusters at a desired level for precipitation hardening later. At the same time, serious segregation of additive elements leading to the formation of coarse particles is prevented. The increase in the solid solubility of a solute in an individual system is a function of cooling rate [39], but for a given cooling range, the relative solubility of various alloying elements is associated with the atomic size [40], electronegativity [41] and electronic structure [42] of the elements.

Table II shows α-phase extension in binary titanium alloy systems due to rapid quenching. A large solubility extension is seen in the types of alloy systems where eutectoid or peritectoid transformation occurs, while almost no extension is realized in the monotectic–peritectoid transformation system. It appears that in such a system, the undercooling of the liquid below the solidus temperature is difficult to attain, due to the large temperature range of the mush zone in the phase diagram. One exception in the solubility extension is that metalloid atoms (carbon or boron) having unfavourable atomic sizes as substitional solutes in titanium undergo extensive dissolution through a different mechanism, i.e. non-substitutional solid solution. In Ti–B alloys, the lattice parameter increases with increasing boron concentration. The appearance of boride particles cannot be seen up to 10 at % B. This evidence suggests that boron atoms may dissolve in the titanium matrix as an interstitial solute [43].

By and large, the experimental results from rapidly quenched titanium binary alloy show that α-phase

TABLE II Comparison of equilibrium and non-equilibrium maximum solid solubility in binary titanium alloys determined from TEM micrographs

Alloy system	Solute concentration in α-phase (at %)	Reference	Phase diagram type	Solution type*	Maximum primary solid solubility	Temperature (°C) and phase
Ti–V	~6	[46]	β-isomorphous	Sub	~3.0	(650, α)
Ti–Mo	<2.0	[46]	β-isomorphous	Sub	0.4	(675, β)
Ti–Fe	~2.5	[46]	Eutectic	Sub	~21	(1085, β)
			Eutectoid		~0.2	(590, α)
Ti–Co	~2.5	[46]	Eutectic	Sub	~14.5	(1020, β)
			Eutectoid		~0.8	(685, α)
Ti–C	~10	[42]	Eutectic		0.55	(1645, β)
			Peritectoid	Int (?)	<0.55	(920, α)
Ti–B	~10	[43]	Eutectic	Int (?)	<~1	(1540, β)
			Peritectoid		0.43	(886, α)
Ti–Si	~6	[47]	Eutectic		~5	(1330, β)
			Eutectoid	Sub	0.67	(850, α)
Ti–Y	~1.0	[48]	Monotectic		0.5	(1355, β)
			Peritectoid	Sub	~0.2	(875, α)
Ti–Ce	~0.6	[49]	Monotectic		~2	(1390, β)
			Peritectoid	Sub	~1	(900, α)
Ti–La	0.3	[48]	Monotectic		~1	(1550, β)
			Peritectoid	Sub	~1	(900, α)

*Sub: substitutional solid solution,
Int: interstitial solid solution.

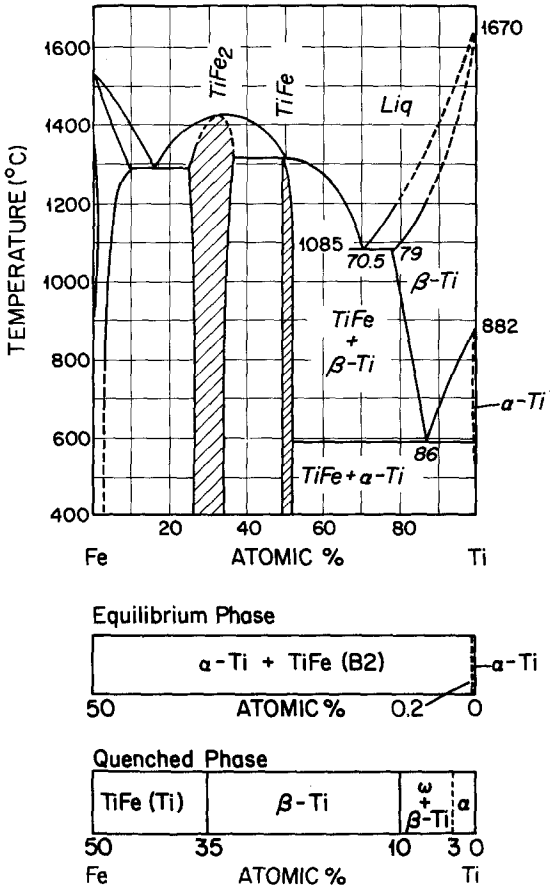

Figure 8 Ti–Fe phase diagram and room-temperature phases by slow cooling and rapid quenching.

extension can be accomplished at the expense of intermetallic compounds, not at the expense of the β-phase, since the occurrence of the ω phase is almost independent of cooling rate and strongly depends upon electron concentration per atom (e/a) [44]. For example, Fig. 8 shows the alloy phases from the equilibrium and rapid-quench phase diagrams [45, 46]. The occurrence of both α-phase extension and a metastable β-phase replaces the TiFe compound phase, but the boundary between metastable α-phase and a metastable β-phase may be associated with electron concentration of the alloy composition.

4.2. Microstructural refinement

Microstructural refinement in rapidly-quenched titanium alloy can be achieved indirectly and directly. The former involves quenching the melt into glassy phases, from which crystalline phases are generated by devitrification and microstructure controlled by means of heat-treatment conditions [50]. Hence, the final microstructures are directly related to the devitrification conditions. Easy glass formation of an alloy is dependent upon phase diagram features (alloy chemical factors) [51, 52], undercooling (nucleation and growth mode factor) [53, 54], and cooling rate (processing factor) [55, 56]. Hence, any comparison of glass-forming properties between two arbitrary compositions requires evaluation of these factors. Typical titanium alloy systems yielding glassy phases include Ti–Ni, Ti–Si, Ti–Cu, Ti–Ni–Si and Ti–Zr–Si (or B) [38, 57, 58]. These glassy phases turn into extremely

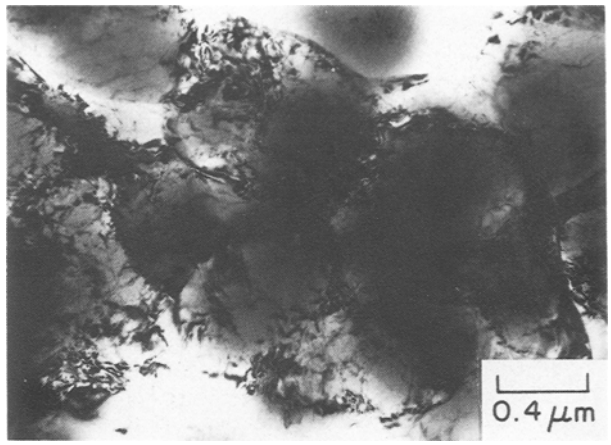

Figure 9 As-splat foil of $TiMn_{10}$ alloy by HA technique.

fine microstructures upon devitrification through appropriate heat treatment [10, 50]. Although devitrified titanium alloys generate extremely fine microstructures and mechanical strength, they contain a large volume fraction of intermetallic compounds or metalloid compounds. To date, bulk alloy processing and applications have not been explored.

Direct refinement has been well recognized in the study of other alloy systems. The dendritic arm spacing [59, 60], eutectic interphase spacing [61] and grain size [62] of as-quenched alloys are power functions of cooling rate, i.e. $\xi = A\dot{T}^{-n}$ where ξ, A, $\dot{T}$ and n are microstructural scale, proportionality constant, cooling rate and characteristic exponent, respectively. From this relationship, conversely, the cooling rate can be estimated by measuring microstructural refinement. Fig. 9 shows typical β-grains in $Ti–Mn_{10}$ after rapid quenching by the HA technique. Measured diameters of the β-grains produced by many different techniques are plotted against the estimated cooling rate in Fig. 10. The correlation line is linear in a

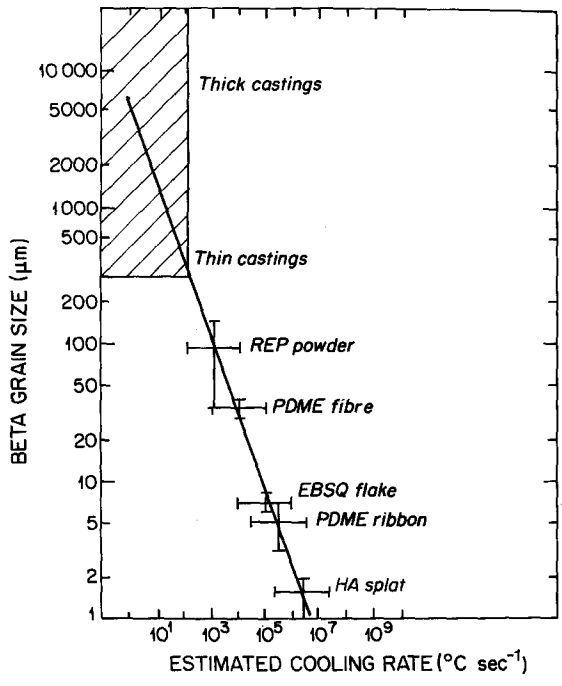

Figure 10 Plot of beta grain size against estimated cooling rate in various titanium alloys [24]. Courtesy of Dr F. H. Froes, Air Force Aeronautical Labs. Slope = −0.4.

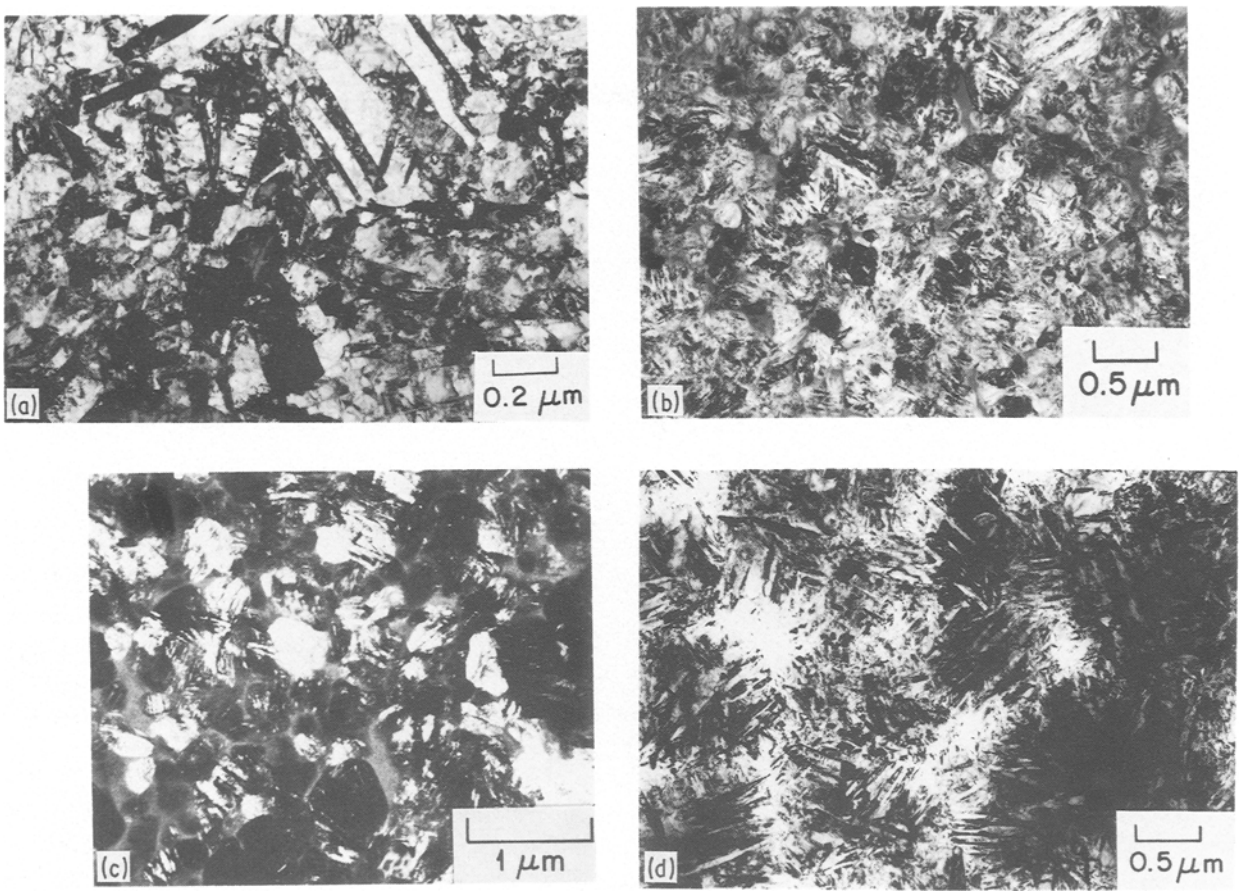

Figure 11 α-phase morphology in as-quenched binary titanium by HA technique: (a) $TiSn_{2.5}$ splat foil, (b) $TiZr_{10}Si_6$ splat foil, (c) dark-field micrograph of (b), (d) $TiNi_{2.5}$ splat foil.

log–normal plot, and has a slope $n = -0.93$ [24]. Hence, the curve in the plot may be expressed as

$$d = A\dot{T}^{-0.93}$$

where d is grain diameter.

In a similar manner, the α-phase also undergoes microstructural refinement upon rapid quenching. α-grains of high aspect ratio are seen in as-quenched $TiSn_{2.5}$ alloy foil (Fig. 11a). In contrast, in $TiZr_{10}Si_6$ alloy foil, refined cellular grains containing very fine martensitic structure are observed in Figs. 11b and c. Another example of refined martensitic structure is shown in Fig. 11d. These refined microstructures are typical examples occurring near titanium-rich terminal compositions.

4.3. Precipitates and dispersoids

In the past, silicide dispersion has been the prime strengthener for high-temperature titanium alloys at elevated temperatures, but below 600° C. The silicides provide good creep strength up to 600° C, but they coarsen rapidly above 600° C, resulting in a reduction in creep strength as well as in post-creep ductility. The dispersion in the silicon-containing titanium alloys is titanium silicide, i.e. the titanium-containing compound. This is Ti_5Si_3 (Hex., $D8_8$) in Ti–Si alloy systems [63, 64] and $(Ti, Zr)_5Si_3$, a pseudo-binary type compound, in the Ti–Zr–(Al)–Si alloy system [1, 2].

In contrast, titanium alloys containing rare-earth metals, which have been processed through rapid solidification, evidence rare-earth dispersion (without titanium) in the as-quenched as well as the annealed state. These dispersoids may be classified into two different types: (i) rare-earth oxides and (ii) intermetallic compounds between rare earth (R. E.) and alloying elements (aluminium, tin etc.). Those dispersoids in binary Ti–R.E. systems were identified as sesquioxide ($R.E._2O_3$) [65], since a significant amount of oxygen is already dissolved in pure titanium. Ternary titanium alloys containing aluminium (or tin) and R.E. were found to contain both oxide and R.E.–Al (or –Sn) intermetallic compounds [35, 38]. Extraction replicas, prepared from Ti–5Al–3La foil annealed at 900° C for 1 h, yield diffraction ring patterns of Al_3La (Hex., Do_{19}) and Al_4La (Orth., DI_3) identified by TEM [48, 66]. Similarly, diffraction ring patterns of Ti–9.5Sn–5.3La alloy after heat treatment at 800° C for 1 h were identified as α-Ti (matrix) and La_2Sn (Hex., $B8_2$) (dispersoids) [48]. Also extraction replicas (Fig. 12) from Ti–10Al–9Er foil were studied by electron microprobe analysis. The microprobe spectra from different particles of the replica show different patterns (as shown in Figs. 12b and c, in which Fig. 12b exhibits spectra of aluminium and erbium, while Fig. 12c shows only erbium [36]), but no oxygen peak was found in the spectra due to the limited sensitivity of the probe to small amounts of oxygen. The dispersoid in $Ti_{89}Al_8Y_3$ alloy treated by laser surface melting was identified as Y_2O_3 by diffraction spot patterns [67]. All these observations lead to the conclusion that both oxide and rare-earth intermetallic compounds coexist in the matrix unless

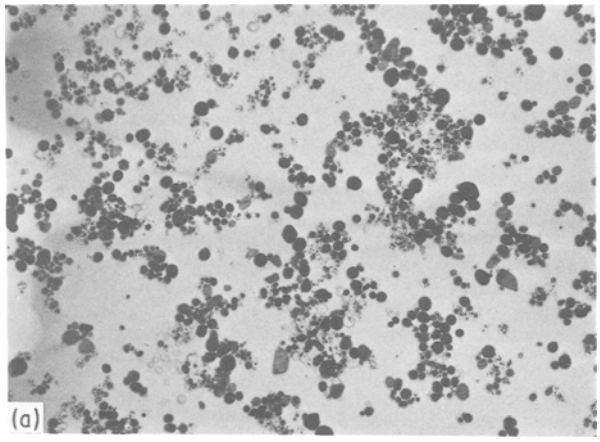

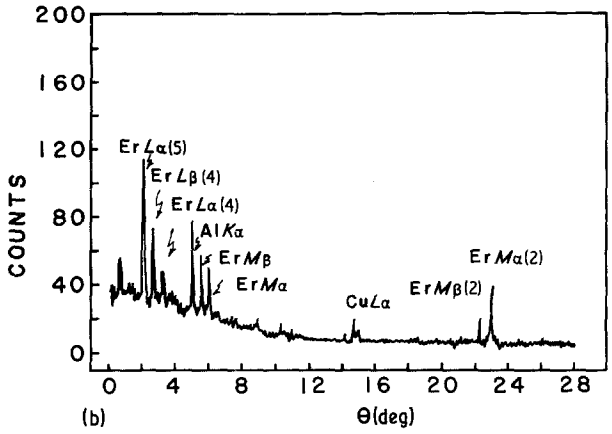

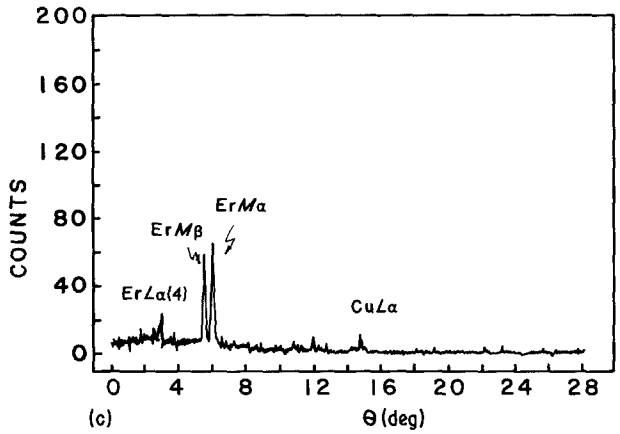

Figure 12 (a) Carbon extraction replica from Ti–5Al–5.4Er alloy annealed at 760° C for 2 h; (b) electron microprobe spectra of carbon extraction replica from Ti–10Al–9Er alloy annealed at 930° C for 36 h; (c) electron microprobe spectra of different particles in the same replica.

titanium is free from oxygen. The oxygen concentration in titanium alloy varies depending upon the starting materials, alloying process, and atmosphere during heat treatment. The fraction of oxide and intermetallic compound phase is determined by phase equilibria in the quaternary phase diagram including oxygen. These quaternary diagrams, however, have not so far been characterized. Table III includes recent findings on the identity of rare-earth dispersoids in titanium alloys. It should be noted that silicides in rapidly solidified titanium alloys take a spherical shape, as opposed to the rod- or needle-shaped silicide precipitates in slowly cooled titanium alloys. The growth of silicide in the highly disturbed matrix containing a high concentration of defects is apparently different from that in the undisturbed matrix.

4.4. Microstructural coarsening

Recently, Ostwald ripening of silicide in rapidly-quenched Ti–5Al–2Si alloy has been studied at 700 and 800° C [6]. Figs. 13a and b show bright-field micrographs of as-quenched Ti–5Al–2Si splat and the coarsened silicide particles after 4 h at 800° C in Ti–5Al–2Si alloys. The measured particle radius is plotted against annealing time in Fig. 14a, and the cube of the radius against time yields a linear correlation (Fig. 14b), indicating that volume-diffusion is the dominant mechanism at these temperatures. From the slope in Fig. 14b, the coarsening rate ($m^3 sec^{-1}$) was determined as listed in Table IV. The diffusivity of the solute (silicon) was calculated on the assumption that the coarsening process is controlled solely by solute, and the volume fraction is assumed according to one of the existing models [69]. The results show that a high coarsening rate is caused by high diffusivity of the silicon solute. A time-invariant distribution function $\varrho^2 h$ (ϱ) [70] was plotted against ϱ, defined as $r/\bar{r}$ where $\bar{r}$ is the average particle radius, as shown in Fig. 15. A significant deviation in size distribution from the Lifshitz–Slyozav–Wagner model [71, 72] at high ϱ values was observed, i.e. the size range in Ti–5Al–2Si is wider than that predicted in the LSW model. Also, the coarsening behaviour of rare-earth particles (La_2Sn) in Ti–5Sn–4.5La was studied by TEM [73]. Figs. 16a and b show micrographs of as-quenched and annealed (800° C for 60 h) Ti–5Sn–4.5La foils. No particle larger than 5 nm diameter can be found in the as-quenched alloy (Fig. 16a).

TABLE III Structure of dispersion in rapidly solidified titanium alloy

Alloy (wt %)	Ageing temperature (° C)	Identified structure	Analytical technique*	Particle shape	Reference
Ti–Zr–Si	500 to 550	$(Ti, Zr)_5 Si_3$, $D8_8$		Equiaxed	[1, 2]
Ti–Y (Ce, Dy, Er, Gd, La, Nd)		R. $E._2O_3$, sesquioxide	TEM, Auger	Circular or rectangular	[65]
Ti–8Al–4Y (at %)	Laser melting	Y_2O_3	TEM	Circular or disc	[67]
Ti–5Sn–3Y	700	Y_5Sn_3 and Y_2O_3	CER, EDXS, EDRP	Circular or rectangular	[68]
Ti–5Al–4.5La	700	Al_3La and Al_4La	CER, EDRP	Circular	[48, 66]
Ti–5Sn–4.5La	700	La_2Sn	EDRP, EELS	Cicular	[48]

*CER: Carbon extraction replica; EDXS: energy-dispersive X-ray spectroscopy; EDRP: electron diffraction ring pattern; EELS: electron energy-loss spectroscopy.

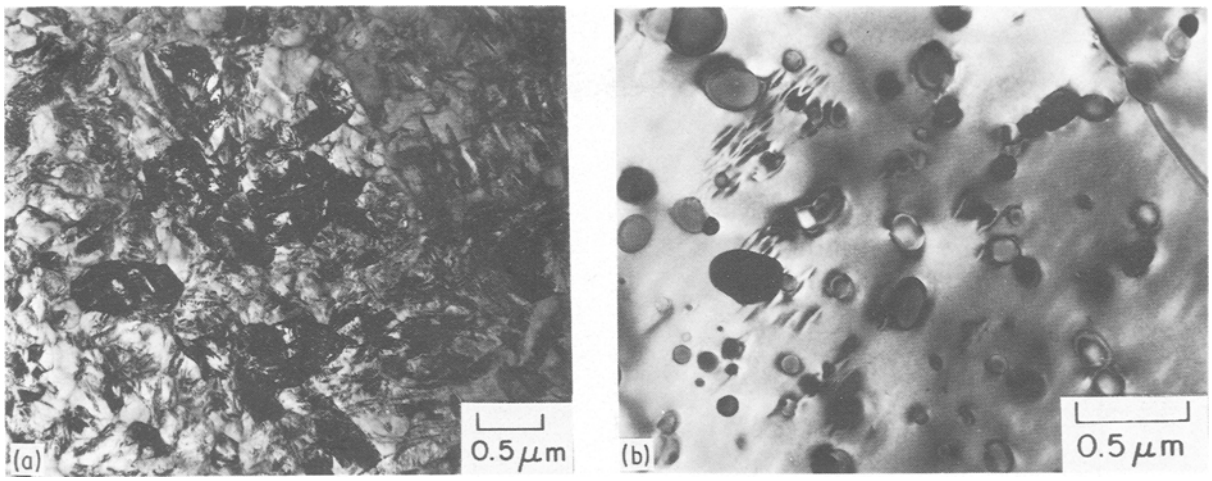

Figure 13 TEM micrographs of Ti–5Al–2Si alloy: (a) as-splat foil by HA technique; (b) the same foil after annealing at 800° C for 4 h.

The radii of the coarsened particles (identified as La_2Sn) are plotted against annealing time at 800° C in Fig. 17. At this temperature, coarsening is again governed by the volume diffusion mechanism. All these measured values and the estimated diffusivities of solutes are tabulated in Table IV. The much slower coarsening rate of lanthanum dispersoids, when compared with silicide in titanium, is very impressive. The estimated diffusivity of lanthanum is three orders of magnitude lower than that of silicon at 800° C. The superior coarsening resistance of lanthanum dispersoids provides high-temperature strength (> 600° C), which will be discussed in the next section.

The effect of rare-earth additions to titanium on the microstructural kinetics has been studied [74]. The addition of yttrium increases the incubation time of recrystallization and decreases the recrystallization rate. In contrast, grain growth kinetics in Ti–Er, Ti–Y and Ti–Al–La [36] show that the time exponent n remains less than 0.5. ($D = kt^n$, where D, K and t are grain diameter, proportionality constant, and annealing time, respectively.) None the less, no apparent effect of rare-earth addition (Ti–Er, Ti–Y) on n value was observed.

5. Mechanical properties

Preliminary investigation has shown the achievement of significant improvement in the mechanical properties of binary and ternary titanium alloy systems processed by RSP. The properties investigated comprise (a) ambient-temperature strength: yield strength, ultimate tensile strength, hardness and elongation, and (b) high-temperature strength: yield strength, ultimate tensile strength, hardness, elongation and creep. Nevertheless, microstructure-sensitive properties such as fatigue and fracture toughness have not been reported on in depth.

5.1. Age-hardening

One of the distinctive phenomena in rapidly solidified titanium alloys containing metalloids and rare-earth metals is age-hardening arising from heat-treatment after rapid quenching from either solution treatment (silicon additive) or from the liquid (all other additives). Details of age-hardening have been reported in liquid-quenched $TiZr_{10}Si_x$, where $x = 2$ to 8 [47]. The results show that a strength increase is attributed to the precipitation of silicide particles. The silicide particles maintain equiaxed shape after coarsening at high temperature. The precipitates take two types of intermetallic compounds: (i) titanium-containing compounds; (ii) non-titanium containing compounds, i.e. rare-earth oxides and rare-earth–simple metal compounds. The degree of supersaturation, cooling rate and additive concentration determines the intensity of ageing. Figs. 18 and 19 show typical ageing behaviour for rare-earth containing alloys upon isothermal annealing and isochronal annealing, respectively. The ageing temperature (~ 700° C) is much higher than that in silicon-containing alloys (~ 500° C). The isochronal annealing experiment confirms the ageing behaviour and over-ageing at high temperatures (800 to 900° C) [36].

5.2. Ambient-temperature strength

When titanium alloys are rapidly quenched and

TABLE IV Determined particle coarsening parameters in RS ternary titanium alloys

Alloy composition	Dispersoid	Total volume fraction of precipitate (%)	Coarsening rate ($m^3 sec^{-1}$)	Estimated diffusivity of solute ($cm^2 sec^{-1}$)	Reference
Ti–5Al–2Si	Ti_5Si_3	~ 8	2.1×10^{-27} (700° C) 3.45×10^{-26} (800° C)	$\sim 7.5 \times 10^{-13}$ $\sim 1.2 \times 10^{-11}$	[6]
Ti–5Sn–4.5La	La_2Sn	1.4	9.4×10^{-29} (800° C)	$\sim 4 \times 10^{-14}$	[73]

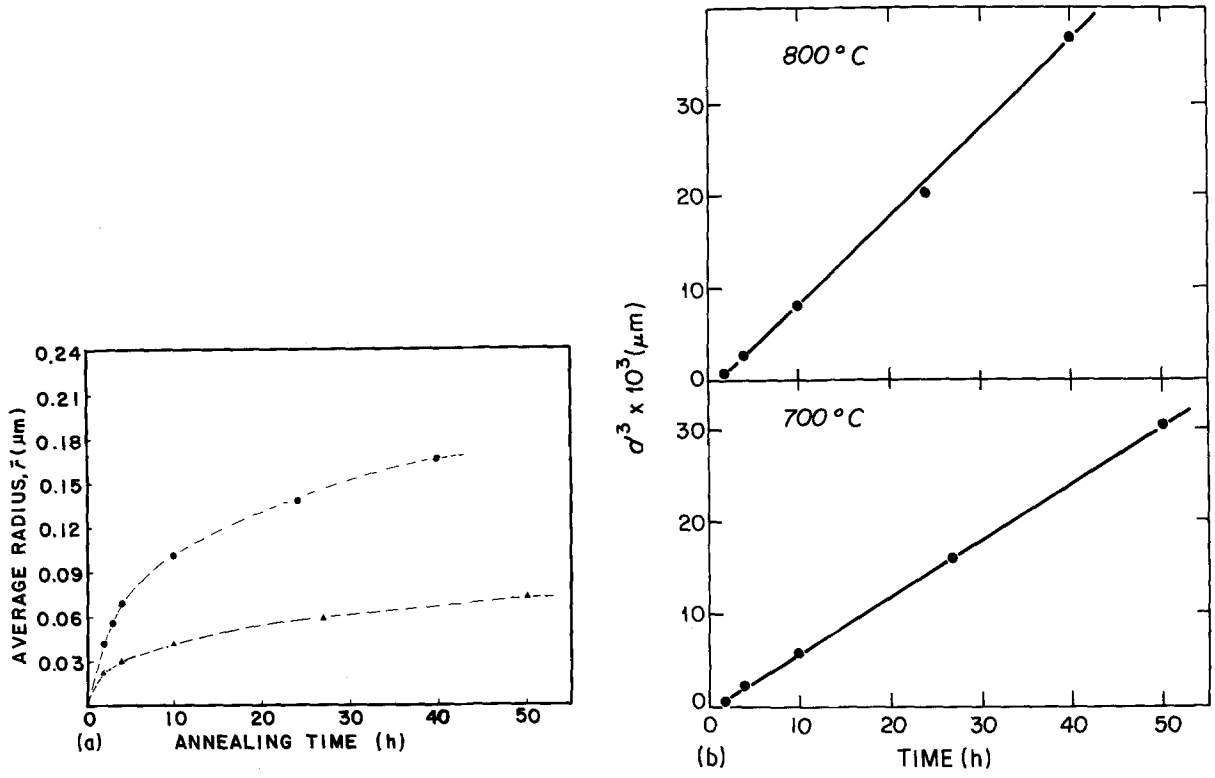

Figure 14 (a) Plot of average silicide particle size as a function of annealing time in Ti–5Al–2Si: (▲) 700° C, (●) 800° C. (b) Plots of cube of average particle radius against annealing time in Ti–5Al–2Si.

consolidated into bulk form, room-temperature strength can increase by as much as 15 to 40% from that of conventional alloys of similar composition processed by ingot metallurgy. Typical examples are given in Table V; these examples demonstrate significant improvements in both strength and elongation as a result of changing the processing technique from ingot metallurgy to RSP. Furthermore, rapid solidification permits the solute least soluble in titanium to dissolve into the titanium matrix, which is not possible through conventional ingot metallurgy. As a result, in rapidly quenched titanium alloys the volume fraction of dispersoids can be controlled at an optimum level. In particular, room-temperature deformation is significantly affected by grain size, the size and volume fraction of dispersoids and the oxygen concentration [75]. The former two parameters are controlled by cooling rate and heat-treatment conditions, while the latter can be minimized by a non-reactive environment during hot processing. Although strength measurements have been carried out on binary and ternary titanium alloy systems, experimentation on fracture toughness and fatigue has to be carried out in order to evaluate the overall impact of RSP on mechanical properties.

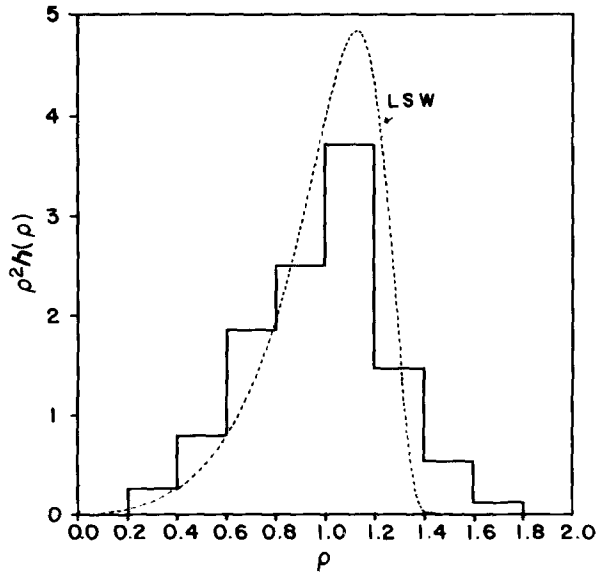

Figure 15 Relative particle size distributions in Ti–5Al–2Si, annealed at 700° C for 27 h.

5.3. High-temperature properties

For high-temperature applications, the temperature dependence of mechanical properties in rapidly solidified titanium alloys have been studied in temperature ranges up to 900° C. The properties invesigated are tensile strength, hot hardness and creep strength. Tensile strength decreases in RS titanium alloys containing rare-earth metals below 600° C as a result of lattice softening and weakening of work-hardening (dislocation dissipation). It is shown that, at 700° C, the ultimate tensile strength decreases nearly to the yield stress (Fig. 20); i.e. there is an absence of work hardening, while grain growth (α-phase) and coarsening of rare earth dispersoids are minimal below 600° C. Fig. 21 shows sharp decreases in microhardness of Ti–5Al–4.5La alloys above 600° C, indicating that the dispersoids are no longer an effective dislocation barrier, probably due to the high diffusitivity of the matrix which in turn increases the creep rate. It appears that at high temperatures (700 to 900° C) the matrix softening of the ternary alloys, which is the prime cause of hardness decrease, does not support the dispersion-strengthening mechanism.

On the other hand, isothermal heat treatment at

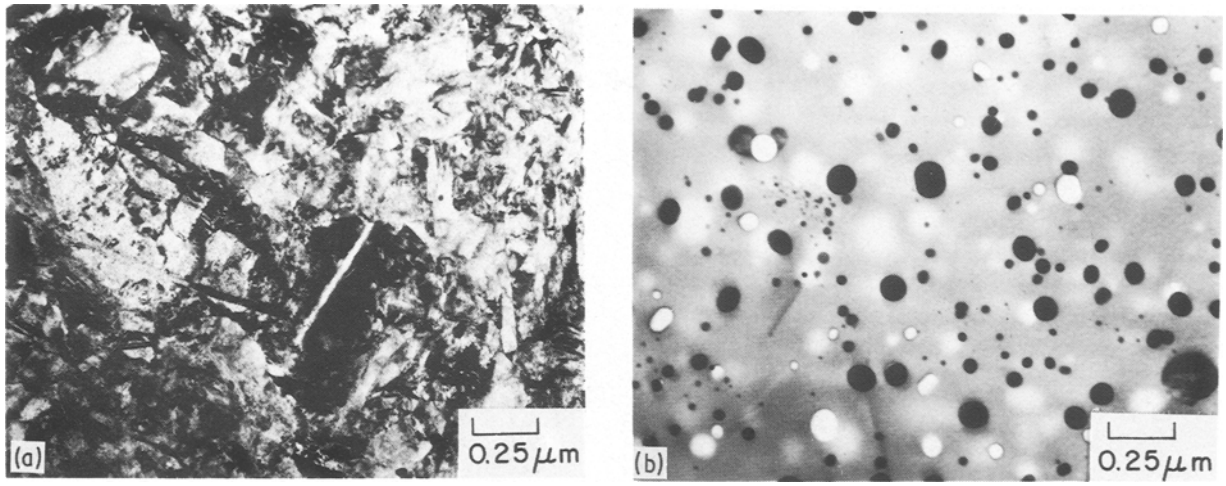

Figure 16 TEM micrographs of Ti–5Sn–4.5La alloy: (a) as-quenched foil by HA technique; (b) the same foil after annealing at 800° C for 60 h.

elevated temperatures (above 600° C) leads to the softening of an alloy (observed at room temperature), which progresses as a function of time resulting from grain growth and particle coarsening. Such an event with Ti–5Al–4.5La alloy undergoing softening during annealing at 900° C is demonstrated in Fig. 22. The calculated Hall–Petch stress (σ_{H-P}) and Orowan–Ashby stress (σ_{O-A}) [76] support the above explanation [36].

Preliminary creep experiments on binary Ti–1.5Nd and Ti–1.0Er reveal that a significant creep-rate reduction is seen at intermediate temperatures (~ 700° C), while a mild improvement is shown in the creep resistance at low temperatures (~ 482° C). Such a discrepancy comes from the fact that the dispersoid does not interact with diffusion creep at low temperatures, but becomes an effective barrier to dislocation creep by pinning dislocation [75].

For a further understanding of the relationships between processing, microstructures and properties in RS titanium alloys, standardized processing methods and subsequent characterization of mechanical properties are desired in the future.

6. Conclusion

Currently, the development of rapidly solidified

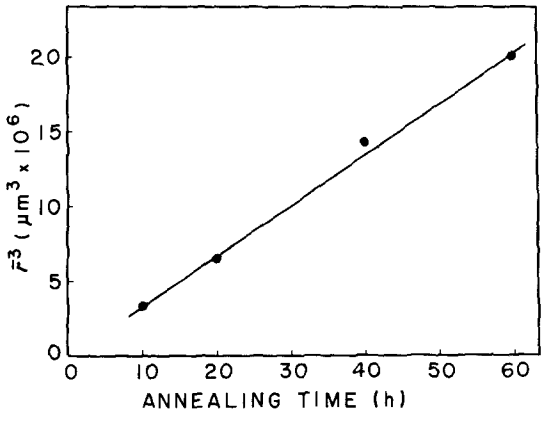

Figure 17 Plot of cube of average particle radius against annealing time at 800° C in Ti–5Sn–4.5La.

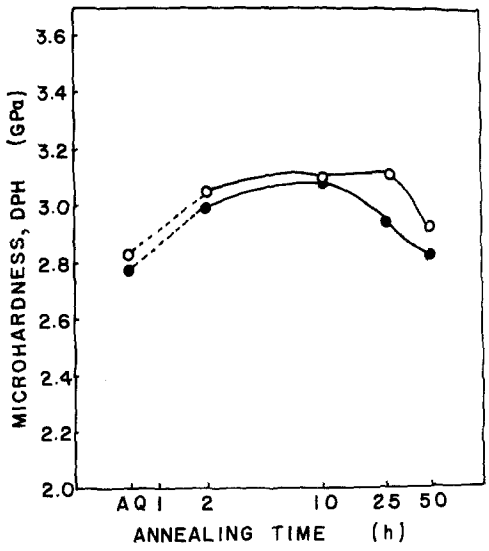

Figure 18 Plot of microhardness against isothermal annealing time at 700° C in (○) Ti–5Al–4.5La and (●) Ti–5Al–5.4Er ribbons. Ribbon thickness 40 μm.

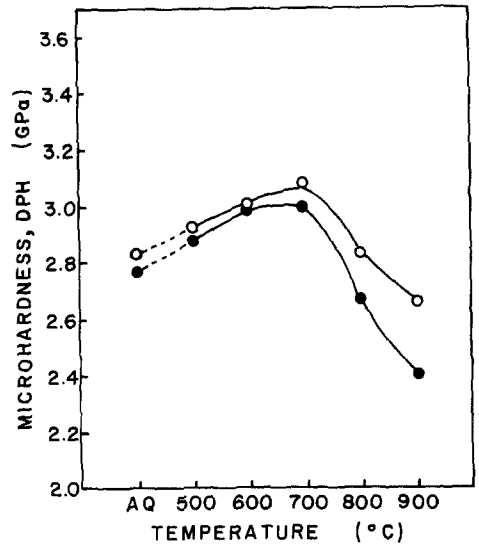

Figure 19 Plot of microhardness against isochronal annealing temperature in (○) Ti–5Al–4.5La and (●) Ti–5Al–5.4Er ribbons. Ribbon thickness 40 μm; annealing time 2 h each.

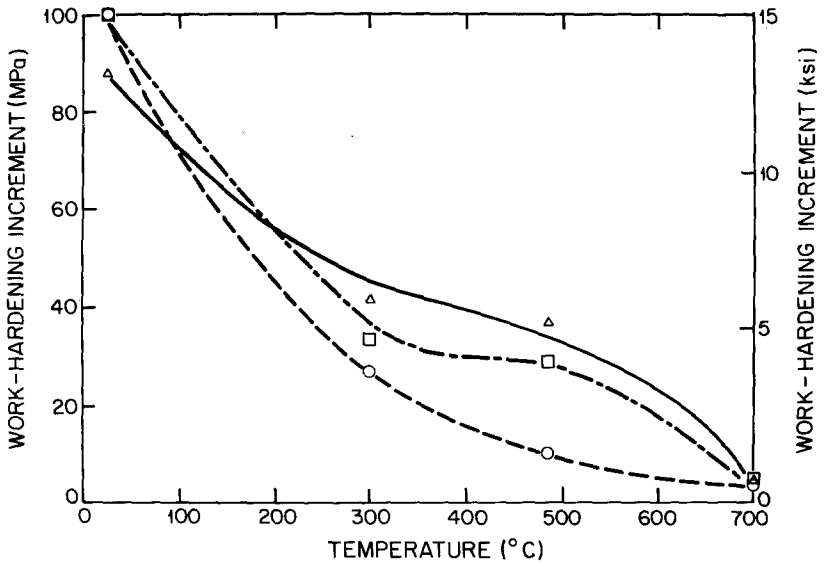

Figure 20 Temperature dependence of work-hardening in titanium and titanium alloys [73]. Work-hardening increment = $\sigma_{UTS} - \sigma_{YS}$. (---) Ti, (-·-) Ti–1.5Nd, (——) Ti–1.0Er.

titanium alloy is confined to the laboratory scale, though it has demonstrated a strong potential for developing into industrialized products. There is no doubt that refinement of rapid soldification processing techniques will likely stimulate more detailed research and eventually lead to industrialized applications. It has been shown that general scientific principles involved in rapid solidification technology are also applicable to titanium alloy systems. As a result, similar benefits deriving from RST are anticipated from RS titanium alloy application. Although only RSP high-temperature α-Ti alloys were discussed in this review, α/β-Ti alloys or β-Ti alloys also can be processed by RST in an effort to improve the desired properties. Research in this area will undoubtedly be opened up in the near future when RS powder processing techniques gain their maturity in parallel with titanium aluminide research.

Acknowledgements

The author gratefully acknowledges the support of the Office of Naval Research for rapidly solidified titanium research (contract no. N00014-82-K 0597). I would like to thank Drs F. H. Froes, S. Krishnamurthy, R. E. Maringer and S. M. L. Sastry for permitting me to cite unpublished materials and providing me with photos for this review. For continuing support of rapidly solidified materials programs I also thank Professor B. C. Giessen and the Barnett Institute of Northeastern University. Finally, thanks as well are due to my colleague Dr S. Nourbakhsh for his critical reading of these manuscripts, and Mrs Jean Catoff for help throughout the preparation of the manuscripts. This is Contribution No. 241 from the Barnett Institute.

References

1. K. C. ANTONE, *Trans. AIME* **242** (1968) 1454.
2. H. M. FLOWER, P. R. SWANN and D. R. F. WEST, *Met. Trans.* **2A** (1971) 3289.
3. N. E. PATON and M. W. MAHONEY, *ibid.* **7A** (1976) 1685.
4. C. G. RHODES, N. E. PATON and M. W. MAHONEY, *J. Metals* **30** (1978) 54.
5. D. EYLON, S. FUJISHIRO, P. S. POSTANS and F. H. FROES, *ibid.* **36** (1984) 55.

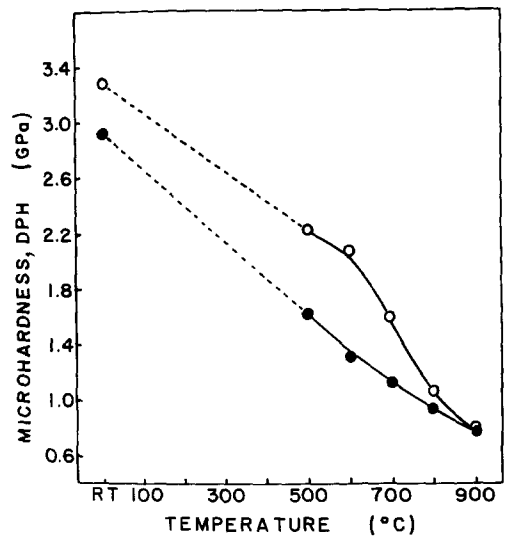

Figure 21 Hot hardness of HIPed (○) Ti–5Al–4.5La and (●) Ti–5Al–5.4Er alloys. Error ± 3%. RT = room temperature.

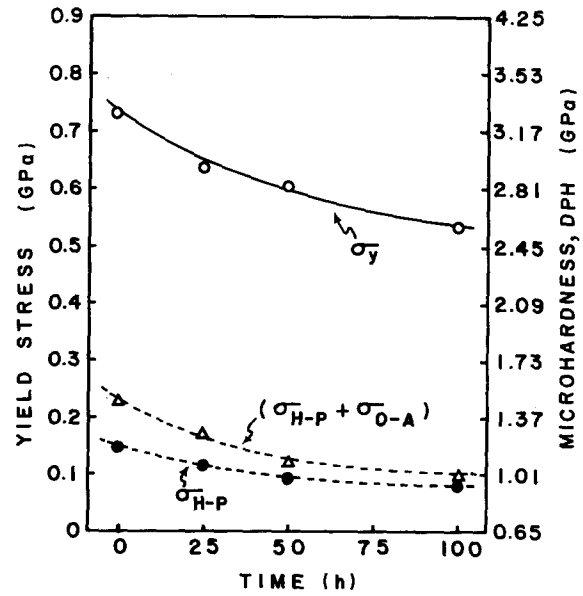

Figure 22 Plot of microhardness (or yield stress) against annealing time at 900° C in Ti–5Al–4.5La alloy. σ_Y is yield stress; σ_{H-P} and σ_{O-A} are calculated Hall–Petch and Orowan–Ashby stresses [36].

TABLE V Comparison of mechanical properties of rapid solidification processed (RSP) and ingot–metallurgical (I/M) Ti–Al–Er alloys [77]

Alloy	Heat treatment*	Yield stress (MPa)		Ultimate tensile stress (MPa)		Total elongation (%)	
		RSP	I/M	RSP	I/M	RSP	I/M
Ti–5Al–2Er	ST	670	469	735	536	27.0	–
Ti–7.5Al–2Er	ST	850	680	920	756	–	7.0
Ti–9Al–2Er	ST	880	750	928	790	11.0	0.1
Ti–5Al–2Er	STA (625° C)	700	510	763	564	13.8	10.0
Ti–7.5Al–2Er	STA (625° C)	952	815	973	843	7.7	6.0
Ti–9Al–2Er	STA (625° C)	931	802	952	824	1.6	0.2
Ti–5Al–2Er	STA (550° C)	714	515	780	590	54.0	18.0
Ti–7.5Al–2Er	STA (550° C)	973	830	990	865	12.0	9.0
Ti–9Al–2Er	STA (550° C)	–	810	–	835	–	0.3

*STA: solution treatment at 860° C for 3 h and water quench;
STA: ST plus ageing at 625° C for 25 h or 550° C for 500 h.

6. S. H. WHANG, Y. Z. LU and B. C. GIESSEN, *Proc. Mater. Res. Soc. Symp.* **28** (1984) 367.
7. J. STRINGER, *Acta Metall.* 8 (1969) 758.
8. P. KOFSTAD, *J. Less-Common Met.* **12** (1967) 449.
9. S. M. L. SASTRY, T. C. PENG, P. J. MESCHTER and J. E. O'NEAL, *J. Metals* **35** (9) (1983) 21.
10. S. H. WHANG, *ibid.* **36** (1984) 36.
11. *Idem*, US Patent 4 512 826 (1985).
12. D. SHECHTMAN, M. J. BLACKBURN and H. A. LIPSITT, *Met. Trans.* **5A** (1974) 1373.
13. C. G. RHODES, C. H. HAMILTON and N. E. PATON, Report AFML–TR–78–130 (1978).
14. H. A. LIPSITT, D. SHECHTMAN and R. E. SCHAFRIK, *Met. Trans.* **11A** (1980) 1369.
15. S. M. L. SASTRY and H. A. LIPSITT, in Proceedings of the 4th International Conference on Titanium, Kyoto, Japan, 19–22 May 1980, edited by H. Kimura and O. Isumi (Metallurgical Society of AIME, 1980) p. 1231.
16. M. J. BLACKBURN and M. P. SMITH, US Patent 4 294 615 (1981).
17. P. L. MARTIN, M. G. MENDIRATTA and H. A. LIPSITT, *Met. Trans.* **14A** (1983) 2170.
18. R. J. KERANS, *ibid.* **15A** (1984) 1721.
19. E. J. CHAPIN and R. LISS, Report of NRL Program (December 1955).
20. B. LOVE, WADE Technical Report No. TR57–666, Part II (March 1959).
21. N. J. GRANT, US Patent 3 070 468 (1962).
22. M. B. VORDAHL, US Patent 3 662 406 (1971).
23. P. R. ROBERTS and P. LOEWENSTEIN, in "Powder Metallurgy of Titanium Alloys", edited by F. H. Froes and J. E. Smugeresky (The Metallurgical Society AIME, Warrendale, Pennsylvania, 1980) p. 21.
24. T. F. BRODERICK, A. G. JACKSON and F. H. FROES, *Met. Trans.* **16A** (1985) 1951.
25. R. E. MARINGER and C. E. MOBLEY, *J. Vac. Sci. Technol.* **11** (6) (1974) 1067.
26. R. E. MARINGER, C. E. MOBLEY and E. W. COLLINGS, *Amer. Inst. Chem. Engnrs* **74** (180) (1978) 111.
27. S. H. WHANG, C. S. CHI and Y. Z. LU, in Proceedings of 5th International Conference on Rapidly Quenched Metals, Würzburg, Germany, 3–7 September, 1984, edited by S. Steeb and H. Warlimont (Elsevier, 1985) p. 115.
28. D. G. KONITZER, K. W. WALTZERS, E. L. HEISER and H. L. FRASER, *Met. Trans.* **15B** (March 1984) 149.
29. S. M. L. SASTRY, T. C. PENG and J. E. O'NEAL, in "Modern Development in Powder Metallurgy", Vols 15 to 17, Proceedings of International Powder Metallurgy Conference, Toronto, June 1984 (Metal Powders Industries Federation, Princeton, NJ).
30. E. W. COLLINGS, R. E. MARINGER and C. E. MOBLEY, Technical Report AFML–TR–78–70 (1978).
31. H. H. LIEBERMANN and C. D. GRAHAM, *IEEE Trans. Magn.* **MAG-12** (1976) 921.
32. S. KAVESH, in "Metallic Glasses", edited by J. J. Gilman and H. J. Leamy (ASM, Metals Park, Ohio, 1976) p. 36.
33. S. H. WHANG and B. C. GIESSEN, NBS Report on Rapid Solidification Processing (National Bureau of Standards, Washington, DC, 1982) p. 439.
34. H. H. LIEBERMANN, *J. Non-Cryst. Sol.* **61/62** (1984) 719.
35. R. C. RUHL, *Mater. Sci. Eng.* **1** (1967) 313.
36. C. S. CHI and S. H. WHANG, in Proceedings of 1985 TMS–AIME Symposium on Rapidly Solidified Materials, edited by S. M. L. Sastry and B. MacDonald, (The Metallurgical Society AIME, Warrendale, Pennsylvania).
37. S. KRISHNAMURTHY, A. G. JACKSON, H. JONES and F. H. FROES, *Mets. Trans. A*, to be published.
38. D. E. POLK, A. CALKA and B. C. GIESSEN, *Acta Metall.*, **26** (1978) 1097.
39. A. K. SINHA, B. C. GIESSEN and D. E. POLK, "Treatise on Solid State Chemistry", Vol. 3, edited by N B. Hannay (Plenum, New York, 1976) p. 1.
40. W. HUME-ROTHERY, G. W. MABBOTT and K. M. CHANNEL-EVAN, *Phil. Trans. R. Soc.* **A 233** (1934) 1.
41. L. DARKEN and R. GURRY, "Physical Chemistry of Metals" (McGraw-Hill, New York, 1952) p. 86.
42. W. HUME-ROTHERY, in "Phase Stability in Metals and Alloys", edited by P. S. Rudman, J. Stringer and R. I. Jaffee (McGraw-Hill, 1967) p. 3.
43. S. H. WANG, Annual Report to the Office of Naval Research, Arlington, Virginia, 1984 (North eastern University, Boston, Massachusetts).
44. E. W. COLLINGS, in "The Physical Metallurgy of Titanium Alloys", (American Society for Metals, Metals Park, Ohio, 1984) Ch. 4.
45. R. RAY, B. C. GIESSEN and N. J. GRANT, *Met. Trans.* **3A** (1972) 627.
46. S. H. WHANG and C. S. CHI, in "Proceedings of the Materials Research Society Meeting on Rapidly Solidified Alloys", 2–17 December 1985, Boston, Mass, edited by B. C. Giessen, D. E. Polk and A. I. Taub (Elsevier) in press.
47. S. H. WHANG, Y. Z. LU and Y. W. KIM, *J. Mater. Sci. Lett.* **4** (1985) 883.
48. C. S. CHI and S. H. WHANG, unpublished work.
49. *Idem*, TMS–AIME paper selection F83–14 (Metallurgical Society AIME, Warrendale, Pennsylvania, 1983).
50. S. H. WHANG and Y. Z. LU, in Proceedings of Rapid Solidification Processing III, (National Bureau of Standards, 1982) p. 286.
51. D. TURNBULL, *J. Phys. (Paris) Colloque C4* **35** (1974) 1.
52. B. C. GIESSEN and S. H. WHANG, *J. Phys. (Paris) Colloque C8* **41** (1980) 95.
53. J. H. PEREPEZKO and J. S. PAIK, in "Rapidly Solidified Amorphous and Crystalline Alloys", edited by B. H. Kear, B. C. Giessen and M. Cohen (Elsevier, New York, 1982) p. 42.
54. W. J. BOETTINGER, *ibid.*, p. 99.
55. D. E. POLK and B. C. GIESSEN, in "Metallic Glasses", edited by J. J. Gilman and J. H. Leamy (ASM, Metals Park,

Ohio, 1978) 1.
56. H. A. DAVIES, in "Rapidly Quenched Metals III" Vol. 1, edited by B. Cantor (The Metals Society, London, 1978) p. 1.
57. S. H. WHANG, *Mater. Sci. Eng.* **57** (1983) 87.
58. *Idem, Scripta Metall.* **18** (1984) 309.
59. W. E. BROWER, R. STRACHAN and M. C. FLEMINGS, *Cast Met. Res. J.* **6** (1970) 176.
60. V. K. SARIN and N. J. GRANT, *Met. Trans.* **8A** (1972) 875.
61. W. KURZ and D. J. FISHER, *Acta Metall.* **28** (1980) 777.
62. P. G. BOSWELL and G. A. CHADWICK, *Scripta Metall.* **11** (1977) 459.
63. H. NOWOTNY, H. AUER-WELSBACH, J. BRUSS and A. KOHL, *Monatsh. Chem.* **90** (1959) 15.
64. L. V. LUZHNIKOR, V. M. NOVIKOVA and A. P. MAREEV, *Metalloved i Term. Obrabotka Metal.* **2** (1963) 13.
65. S. M. L. SASTRY, P. J. MESCHTER and J. E. O'NEAL, *Met. Trans.* **15A** (1984) 1451.
66. C. S. CHI and S. H. WHANG, *Proc. Mater. Res. Soc. Symp.* **28** (1984) 356.
67. D. G. KONITZER, B. C. MUDDLE and H. L. FRASER, *Met. Trans.* **14A** (1983) 1979.
68. Y. Z. LU and S. H. WHANG, in "Proceedings of the Materials Research Society Meetings on Rapidly Solidified Alloys", 2–17 December, 1985, Boston, Mass., edited by B. C. Giessen, D. E. Polk and A. I. Taub (Elsevier) in press.
69. A. J. ARDELL, *Acta Metall.* **20** (1972) 61.
70. A. J. ARDELL and R. B. NICHOLSON, *J. Phys. Chem. Solids* **27** (1966) 1793.
71. I. M. LIFSHITZ and V. V. SLYOZAV, *ibid.* **19** (1961) 35.
72. C. WAGNER, *Z. Elecktrochem.* **65** (1961) 581.
73. Y. Z. LU, C. S. CHI and S. H. WHANG, in Proceedings of 5th International Conference on Rapidly Quenched Metals, 3–7 September 1984, Würzburg, Germany, edited by S. Steeb and H. Warlimont (Elsevier, 1985) p. 949.
74. B. B. RATH, B. A. MACDONALD, S. M. L. SASTRY, R. J. LEDERICH, J. E. O'NEAL and C. R. WHITSETT, in "Titanium '80", Vol. 2, edited by H. Kimura and O. Isumi, 19–22 May 1980, Kyoto, Japan (AIME, 1980) p. 1185.
75. S. M. L. SASTRY, T. C. PENG and L. P. BECKERMAN, *Met. Trans.* **15A** (1984) 1465.
76. M. F. ASHBY, in Proceedings of 2nd Bolton Landing Conference on Oxide Dispersion Strengthening, edited by G. S. Ansell (Gordon and Breach, 1968) p. 143.

Received 23 October
and accepted 13 November 1985